APPLICATION OF THE VARIATIONAL METHOD OF TOVS DATA OVER THE TIBETAN PLATEAU IN IMPROVEMENT OF THE INITIAL FIELD OF NUMERICAL MODELS*

WENG Yonghui (翁永辉), *XU Xiangde* (徐祥德), *BAI Jingyu* (柏晶瑜)

Chinese Academy of Meteorological Sciences, Beijing 100081

and *DONG Chaohua* (董超华)

National Satellite Meteorological Center, Beijing 100081

Received March 6, 2001

ABSTRACT

In this paper, TOVS satellite data are used through variational method on the data-sparse plateau area. Diagnoses are carried out to find a way to solve the large error problem of model initial field. It is put forward that TOVS retrieval data can be used to improve the initial field of numerical prediction model on Tibetan Plateau area. Through variational method, TOVS data are processed and the liability of the initial information on the plateau is improved. Diagnostic results confirm further that the application of TOVS retrieval data can improve our capability to describe the dynamic system features on the plateau and the objectivity of related initial information such as the distribution of water vapor channel and stratification stability.

Key words: TOVS retrieval data, variational method, Tibetan Plateau

I. INTRODUCTION

The Tibetan Plateau has an averaged altitude above the sea level of about 4500 m, with an area of more than 2 000 000 km^2. It is the highest, largest plateau with the most complex terrain. With the establishment of meteorological observing network in plateau area and the development of meteorological operation and application studies, the weather analyses and numerical prediction are promoted greatly. However, diagnosing the weather and climate on plateau area meets lots of problems difficult to get over, one of which is data problem. This is also the most difficult problem for numerical model applied on the Tibetan Plateau. The observing stations are very few on the plateau. In the 125 radiosonde stations issued by China Meteorological Administration in September 1990, there are only 4 stations in Tibet including Nagqu, Lhasa, Tingri and Qamdo. Furthermore, these 4 stations are all located in the southeast part of Tibet. There are no radiosonde stations in mid-west Tibetan Plateau. Thus, any objective analysis method does not work well for this area. Chen and Qian (1995) found that significant errors exist

* Supported by the National Key Project B-"Observation and Theoretical Study of the Physical Process of the Tibetan Plateau Land-Air Interaction and Its Impact on the Global Climate and Severe Weather in China."

in the western area in the wind and relative humidity field of FGGE obtained in 1979. Especially the relative humidity at various levels is apparently high. To overcome the data-sparse problem in western plateau, based on the statistics on the temporal and spatial correlation of data obtained from the temporary stations, the data obtained from the middle plateau are used to fit western data and then adopted in objective analyses, or the previous data are used to fit later data to compensate data lack on Tibetan Plateau area. In the meantime, satellite data are also considered. As a result, the initial relative humidity field on the Plateau is improved partially with the forecast result improved.

Although the retrieved remote sensing data are not completely the same as the cenventional data, adding some of this kind of data into the conventional data can after all capture some information of mesoscale circulation. By this way, Zhang and Michael (1986) did succeed in simulating the Johnstown flood in 1977. The application of TOVS (the American TIROS-N series operational satellite vertical monitor) data can solve the data-sparse problem to a certain degree. As forecast by Bengtsson (see Wang 1995), no matter from the aspect of practice or economy, it is not easy to provide data that can cover hemisphere or the whole globe by conventional way. Consequently, satellite monitoring will gradually become the main part of global observing system. However in recent practice, the negative effect of the satellite retrieval temperature on the operational numerical weather prediction in Northern Hemisphere is difficult to eliminate. That is because that there is rather good conventional observing network, which can provide high quality initial fields for numerical weather prediction. The forecast accuracy has been rather high (the temperature error for the free air under 150 hPa is less than 2℃). The satellite retrieval data with lower accuracy may play a negative role in data assimilation process. Things are different for the plateau area, where the stations are very sparse with few data obtained. This problem leads to the bad objectivity of objective analysis. Especially in western area, the distance between the stations is about several thousand kilometers. The resolution is very low. Great difficulty exists in the objective analyses there. For the initial field of numerical model, only FGGE data are used, even which still have the problem of large error and less objectivity. In recent years, with the development of satellite operation, TOVS data are having high horizontal, vertical and temporal resolution on plateau area. The retrieving points on plateau are very dense. Thus, TOVS retrieval data will play an important role in the numerical weather prediction on plateau area.

The application of TOVS retrieval data greatly increases the spatial density of data on plateau area.

Through the correction with variational method, the accuracy of TOVS retrieval data is improved also. It is confirmed further that the application of TOVS retrieval data can improve our capability to describe the dynamic system features on the plateau and the objectivity of related initial information such as the distribution of water vapor channel and stratification stability.

II. PRINCIPLE OF VARIATIONAL TECHNIQUE

According to the variational principle, the objective function depending on multi-variables has the following form:

$$J[U(x,y)]=\iint_G F\left(x,y,U,\frac{\partial U}{\partial x},\frac{\partial U}{\partial y}\right)\mathrm{d}x\mathrm{d}y, \tag{1}$$

where $U(x,y)$ must satisfy the following Euler equation:

$$Fu-\left(\frac{\partial}{\partial x}Fu_x+\frac{\partial}{\partial y}Fu_y\right)=0. \tag{2}$$

The employed variational method is the technique used by Xu et al. (1996) to assess the precipitation by combination of satellite with radar data in the study of typhoon and heavy rain disastrous weather monitoring and forecasting techniques, which is a national key project in the 8th National Five-Year Plan.

Let $\tilde{T}^*(x,y)$ be the element field of the TOVS retrieval data, the relevant radiosonde observation field is $Ra(I,J)$, the difference field between above two types of data at the radiosonde observation coordinate (I,J), namely the error filed is represented by $\tilde{C}r(I,J)$:

$$\tilde{C}r(I,J)=Ra(I,J)-\tilde{T}^*(I,J). \tag{3}$$

In fact, since the number of the radiosonde stations (I,J) is limited, it is necessary to construct a more general correction factor field function $Cr(x,y)$. With variational method, the following conditions have to be satisfied to get a $Cr(x,y)$ function:

$$J^*=\iint_D(Cr-\tilde{C}r)^2\mathrm{d}x\mathrm{d}y\to\min, \tag{4}$$

namely $\sum_i\sum_j(Cr-\tilde{C}r)^2$ reaches the minimum value.

For above variational problem, it can be taken as constructing the following objective function J^*

$$J^*=\iint\left\{(Cr-\tilde{C}r)^2+\lambda\left[\left(\frac{\partial Cr}{\partial x}\right)^2+\left(\frac{\partial Cr}{\partial y}\right)^2\right]\right\}\mathrm{d}x\mathrm{d}y=0, \tag{5}$$

where λ is the constraint coefficient. Formula (5) can be rewritten as

$$\delta J^*=\delta\sum\sum\left[(Cr-\tilde{C}r)^2+\lambda\left[\left(\frac{\partial Cr}{\partial x}\right)^2+\left(\frac{\partial Cr}{\partial y}\right)^2\right]\right]=0. \tag{6}$$

The corresponding Euler equation is

$$(Cr-\tilde{C}r)-\tilde{\lambda}\left(\frac{\partial^2 Cr}{\partial x^2}+\frac{\partial^2 Cr}{\partial y^2}\right)=0, \tag{7}$$

where $\tilde{\lambda}$ is the deformation constraint coefficient. The solution of this equation can be obtained through iteration method. Then a new variational correction factor field $Cr(x,y)$ can be obtained. Finally the TOVS retrieval element field after variational correction is

$$T(x,y)=\tilde{T}^*(x,y)+Cr(x,y). \tag{8}$$

III. THE VARIATIONAL CORRECTION EFFECT OF TOVS DATA ON PLATEAU AREA

To verify the feasibility of TOVS retrieval data correction through variational method, experiments are carried out with conventional data and TOVS retrieval data, choosing Nagqu and Lhasa as the experiment targets. Namely, these two stations are not

used as the information sources in the objective analysis process. The experiment schemes are: (1) Cressman analysis scheme. Reject the radiosonde data of Lhasa and Nagqu and analyze other radiosonde data to these two stations to give the Cressman analysis value; (2) TOVS analysis scheme. Analyze TOVS retrieval data with Cressman analysis method to the two stations to give TOVS analysis value; (3) C-TOVS analysis scheme. Reject the radiosonde data at Lhasa and Nagqu, other radiosonde data are used to correct TOVS data through variational method, and analyze the corrected TOVS data to the two stations with Cressman analysis method to give the corrected TOVS value. The variational corrected results of the temperature and horizontal velocity at Nagqu and Lhasa from 0800 BT 6 July to 0800 BT 7 July 1995 are listed in Tables 1—6.

Table 1. Effect of the Variational Corrected TOVS Data at Nagqu at 0800 BT 6 July 1995

		500 hPa	400 hPa	300 hPa	250 hPa	200 hPa	150 hPa	100 hPa
Temperature	Sounding	−2.2	−12.3	−25.8	−35.0	−48.7	−60.9	−70.9
	Cressman	−6.1	−13.2	−28.9	−36.3	−47.6	−57.3	−66.6
	TOVS	−0.1	−11.8	−28.8	−37.1	−48.5	−58.7	−67.9
	C-TOVS	−2.5	−11.8	−27.5	−35.5	−47.4	−58.3	−68.5
Horiziontal velocity	Sounding	13.0	11.0	15.0	19.0	26.0	18.0	13.0
	Cressman	6.6	8.8	19.7	22.6	27.4	18.7	15.4
	TOVS	1.9	4.1	10.5	12.7	11.8	7.2	7.3
	C-TOVS	7.9	7.5	19.0	20.7	26.5	18.3	14.8

Table 2. Effect of the Variational Corrected TOVS Data at Lhasa at 0800 BT 6 July 1995

		500 hPa	400 hPa	300 hPa	250 hPa	200 hPa	150 hPa	100 hPa
Temperature	Sounding	−2.9	−13.8	−27.7	−36.0	−49.5	−60.0	−75.6
	Cressman	−5.0	−12.4	−28.8	−36.6	−48.0	−58.4	−68.4
	TOVS	1.7	−11.1	−26.9	−36.1	−48.6	−60.0	−72.5
	C-TOVS	0.4	−10.8	−25.6	−34.5	−47.3	−59.5	−73.2
Horiziontal velocity	Sounding	7.0	15.0	14.0	16.0	20.0	16.0	8.0
	Cressman	3.5	6.4	15.6	18.0	20.1	14.8	12.8
	TOVS	3.8	10.6	17.4	20.2	21.8	22.8	13.1
	C-TOVS	3.3	6.1	15.6	18.0	20.1	16.1	12.8

Table 3. Effect of the Variational Corrected TOVS Data at Nagqu at 2000 BT 6 July 1995

		500 hPa	400 hPa	300 hPa	250 hPa	200 hPa	150 hPa	100 hPa
Temperature	Sounding	1.6	−10.8	−24.5	−33.5			
	Cressman	−2.0	−13.6	−25.7	−33.8	−43.5	−56.9	−70.3
	TOVS	3.6	−11.1	−26.4	−35.4	−45.8	−57.8	−71.4
	C-TOVS	2.0	−9.9	−25.2	−33.5	−46.9	−60.4	−73.3
Horiziontal velocity	Sounding	7.0	12.0	17.0	18.0			
	Cressman	3.3	6.5	14.5	18.7	24.1	20.1	14.2
	TOVS	4.3	7.3	14.5	18.2	16.0	7.8	10.1
	C-TOVS	8.8	12.0	16.6	15.5	16.9	12.3	12.2

Table 4. Effect of the Variational Corrected TOVS Data at Lhasa at 2000 BT 6 July 1995

		500 hPa	400 hPa	300 hPa	250 hPa	200 hPa	150 hPa	100 hPa
Temperature	Sounding	1.2	−10.1	−23.1	−33.9	−45.9	−60.7	−75.5
	Cressman	−0.7	−11.2	−25.3	−32.0	−47.2	−62.1	−73.9
	TOVS	4.0	−10.0	−25.5	−35.7	−47.9	−61.4	−73.0
	C-TOVS	2.5	−9.1	−24.6	−32.9	−46.4	−61.0	−73.0
Horiziontal velocity	Sounding	6.0	9.0	14.0	9.0	11.0	13.0	12.0
	Cressman	11.2	12.7	13.6	10.7	12.0	16.0	14.1
	TOVS	4.7	6.7	10.7	13.0	13.3	9.5	4.9
	C-TOVS	11.0	10.8	13.6	12.2	12.1	16.0	13.7

Table 5. Effect of theVariational Corrected TOVS Data at Nagqu at 0800 BT 7 July 1995

		500 hPa	400 hPa	300 hPa	250 hPa	200 hPa	150 hPa	100 hPa
Temperature	Sounding	−2.2	−12.3	−27.5	−35.5	−47.2	−59.0	−71.6
	Cressman	−3.1	−13.2	−27.7	−36.3	−45.9	−57.0	−70.3
	TOVS	0.1	−11.7	−28.1	−36.7	−48.4	−60.6	−74.8
	C-TOVS	−1.9	−11.9	−27.1	−35.4	−47.1	−59.0	−71.7
Horiziontal velocity	Sounding	1.0	9.0	22.0	24.0	22.0	25.0	6.0
	Cressman	4.5	4.2	13.6	19.9	24.5	26.9	9.7
	TOVS	3.5	7.9	17.2	22.7	25.1	21.6	12.2
	C-TOVS	1.5	8.4	19.0	22.2	19.9	22.4	5.1

Table 6. Effect of the Variational Corrected TOVS Data at Lhasa at 0800 BT 7 July 1995

		500 hPa	400 hPa	300 hPa	250 hPa	200 hPa	150 hPa	100 hPa
Temperature	Sounding	−1.7	−10.1	−24.1	−32.2	−43.9	−56.7	−70.0
	Cressman	−2.5	−12.3	−26.5	−35.6	−46.5	−58.0	−71.2
	TOVS	0.8	−10.6	−26.8	−35.2	−47.2	−60.2	−74.7
	C-TOVS	−1.4	−10.1	−24.4	−32.2	−44.2	−57.5	−71.2
Horiziontal velocity	Sounding	2.0	5.0	8.0	16.0	15.0	16.0	10.0
	Cressman	2.6	4.0	10.7	15.6	20.2	22.7	8.2
	TOVS	5.2	6.2	11.9	15.9	19.5	21.8	21.8
	C-TOVS	2.8	4.4	7.8	13.2	15.7	20.2	2.7

From Tables 1 — 6, we can see that Cressman analysis can generally capture characteristics of various elements on the Tibetan Plateau. The error of TOVS analyses is larger for the following two reasons. Firstly, compared to the time of radiosonde observation, the time of TOVS retrieval data is a period of time, which may be a source of system error. Secondly, there is error in the TOVS data itself; Compared to above two kinds of analysis data, C-TOVS analysis is closer to radiosonde observation. The differences between the radiosonde observation and the TOVS as well as C-TOVS analysis data at 0800 BT 7 July 1995 are shown in Fig. 1.

Above analyses and comparisons show that Cressman analysis method can be used in the plateau area. Besides, the TOVS data corrected by variational method (i. e. C-TOVS) is much closer to the real data than that without correction. The effect of variational correction is very significant.

IV. NUMERICAL EXPERIMENTS ON RAINFALL

With T63 analysis data, radiosonde data and TOVS retrieval data, MM5 model is employed to carry out 24 h comparison experiments with 0800 BT 5 July 1995 and 6 July 1995 as the initial times. In experiment RAOB, simulation is carried out with T63 and radiosonde data as the initial data. In experiment C-TOVS, the corrected TOVS data are added to the initial field of Exp. RAOB. For the experiment initiated from 0800 BT 5 July 1995, the rainfall location and the rainfall centers are generally the same as the real one (figure omitted). However, the rainfall intensities are different for different schemes. Table 7 gives the comparison among the intensities at three rainfall centers located at Litang, Lhasa and Xigazê.

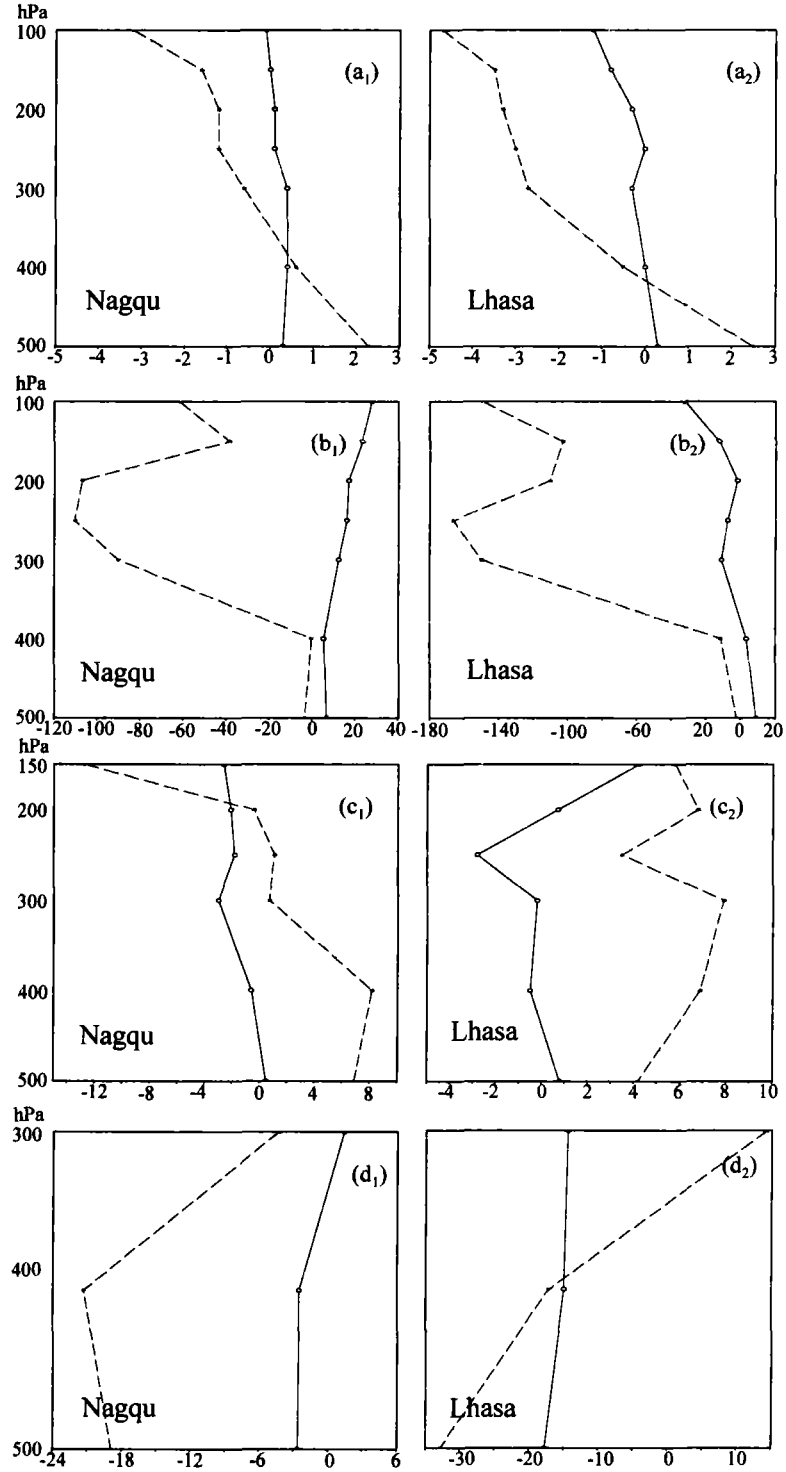

Fig. 1. The differences between the TOVS data and the radiosonde observation at about 0800 BT 7 July 1995. Solid lines denote the TOVS data minus radiosonde data; and dotted lines denote C-TOVS data minus radiosond data. (a_1), (a_2) temperature (°C); (b_1), (b_2) geopotential height (gpm); (c_1), (c_2) horiziontal velocity (m s^{-1}); (d_1), (d_2) relative humidity (%).

Table 7. Comparison of Simulated Rainfall (0800 BT 5 July — 0800 BT 6 July 1995)

	Observation	Experiment RAOB (mm)	Experiment C-TOVS (mm)
Litang	16	114.0	25.8
Lhasa	19	65.8	39.0
Xigazê	18	42.5	35.7
Average error		56.4	15.8

In the experiment initiated at 0800 BT 6 July 1995, the two real rainfall centers at Ya'an and Lhasa do appear in both schemes. However, the simulated positions for Ya'an all deviate to the west by about 3 degrees of longitude, which is near Litang. The rainfall intensity is shown in Table 8.

Table 8. Comparison of the Simulated 24 h Rainfall (0800 BT 6 July—0800 BT 7 July 1995)

	Observation	Experiment RAOB (mm)	Experiment C-TOVS (mm)
Ya'an	34	98.7	39.9
Lhasa	20	38.0	37.0
Average error		41.4	11.5

V. DIAGNOSTIC ANALYSIS

1. *Analyses on the Weather Systems on the Plateau Area*

On the 500 hPa flow field at 0800 BT 5 July 1995, which is obtained from Exp. RAOB (Fig. 2a), there is a weak low vortex on eastern plateau (33°N, 100°E) and a stronger one on the western part (31°N, 84°E). The northern plateau is controlled by anticyclone. Besides, strong southerly wind dominates from Bay of Bangle to southern plateau area. At 2000 BT (figure omitted), the low on the east disappears. The western one gets weakened and moves to the east by two degrees of longitude. The northern anticyclone shifts to the middle plateau and gets weakened. The southern southerly flow deviates to the west. At 0800 BT 6 July 1995, the western low disappears. The middle plateau is controlled by weak anticyclone and low vortex. The southerly wind on the southern plateau turns into southeasterly wind. At 0800 BT 7 July 1995, the middle plateau is controlled by strong low vortex. On the 500 hPa flow field of C-TOVS scheme, at 0800 BT 5 July 1995 (Fig. 2b), the east low is rather strong, the west one is weaker. The deformation field dominates the southern plateau, to the south of which there is southwesterly wind penetrating into the plateau. At 2000 BT 5 July 1995 (figure omitted), the east low disappears. An anticyclone forms on the southern part. At 0800

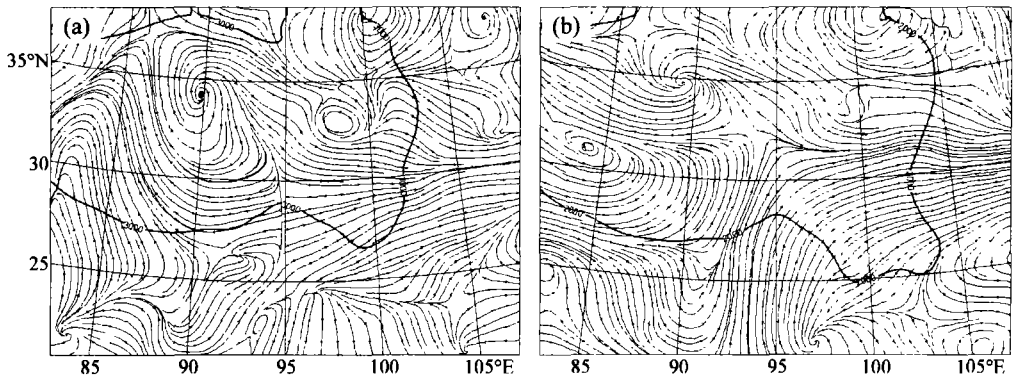

Fig. 2. 500 hPa flow field at 0800 BT 5 July 1995 according to (a) RAOB scheme. and (b) C-TOVS scheme.

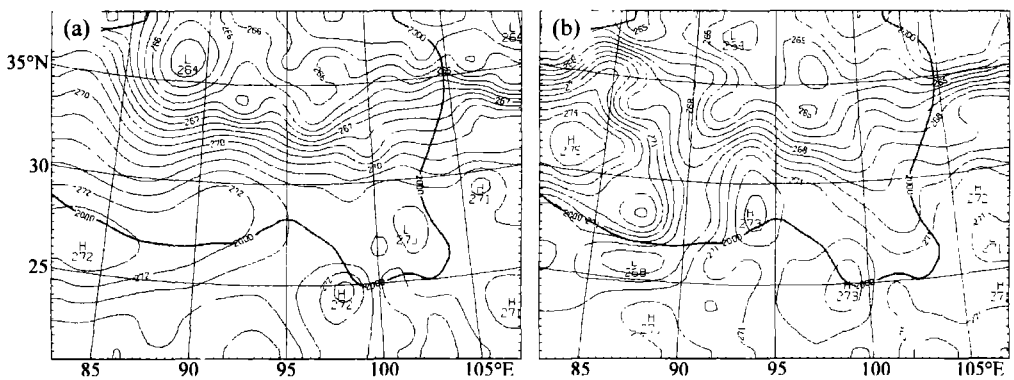

Fig. 3. 500 hPa temperature field at 0800 BT 5 July 1995 according to (a) RAOB scheme and (b) C-TOVS scheme .

BT 6 July 1995, two low vortices form on the east (31°N, 99°E) and middle (33°N, 92°E) parts of the plateau. The weak southwesterly wind on the southern plateau turns into westerly wind. At 0800 BT 7 July 1995, the southeastern and southern parts of the plateau are dominated by rather weak low vortex. On the temperature field at 0800 BT 5 July 1995 of scheme RAOB (Fig. 3), two branches of strong warm-moist flow from the southwest and the south merge at Litang area. In the analyses of C-TOVS scheme, since there is a cold air tongue at 90°E, which cuts off the transportation channel of warm-moist air from the west to Litang, the water vapor transportation at Litang weakens significantly.

These results show that TOVS data can increase the spatial resolution of data on the plateau area. Its application can be an efficient way to overcome the problem of data lack and low spatial data resolution.

2. *The Characteristics of Water Vapor Transportation*

As we know, water vapor flux means the amount (gram) of water vapor that crosses a unit area in unit time period, and represents the amount and direction of water vapor

transportation. The horizontal water vapor transportation is $\boldsymbol{V} \cdot q/g$, the unit is $g\ s^{-1}\ cm^{-1}\ hPa^{-1}$ (see Zhu et al. 1992). Figure 4a shows the water vapor flux field on 400 hPa at 0800 BT 5 July 1995 according to scheme RAOB. From this figure, we can see that there is a strong water vapor channel from Bay of Bangel to the southeastern plateau. Besides, there is another significant water vapor channel from the southwest to southeast part of the plateau. Above two channels meet near Litang and move to the east. Figure 4b shows the 400 hPa water vapor flux field according to scheme C-TOVS, in which there are still two water vapor channels towards eastern plateau. One is from Bay of Bangle, which is rather weak and does not reach the inner part of the plateau. It only transports the water vapor from the southern plateau to the east. The other one is from the northwest. From the velocity field (Fig. 5), we can see that there are two strong wind belts from the south and southwest according to scheme RAOB, while there is only one strong wind belt from Litang to the east according to scheme C-TOVS.

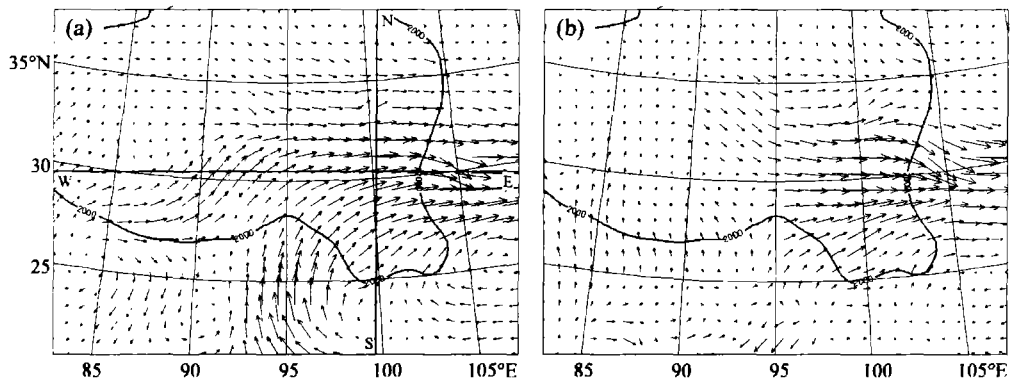

Fig. 4. The 400 hPa water vapor flux field ($g\ kg^{-1} m\ s^{-1}$) at 0800 BT 5 July 1995 according to (a) RAOB scheme and (b) C-TOVS scheme.

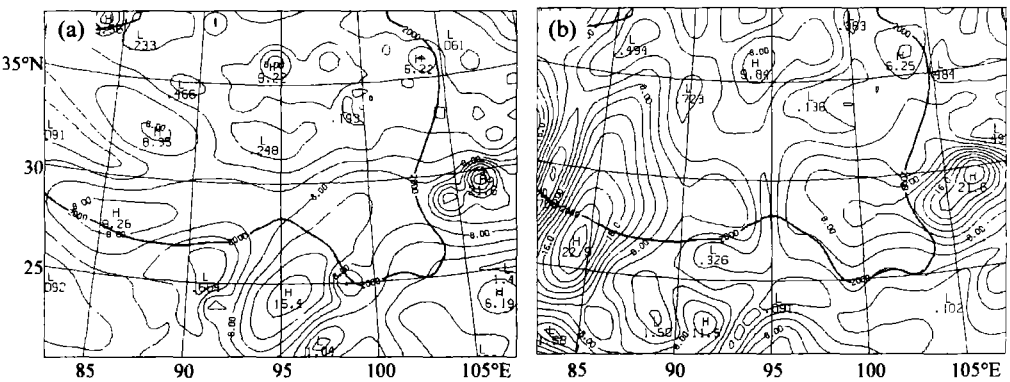

Fig. 5. The 400 hPa velocity field ($m\ s^{-1}$) at 0800 BT 5 July 1995 according to (a) RAOB scheme and (b) C-TOVS scheme.

Figures 6b and 6d show the water vapor cross section from the east to the west along the rainfall center at Litang at 0800 BT 5 July 1995. From the figure, we can see strong water vapor flux towards the north in scheme RAOB and weaker water vapor flux towards the south in scheme C-TOVS. Figures 6a and 6c show the water vapor cross section from the south to the north along the rainfall center at Litang at the same time as that in Fig. 6. The water vapor fluxes are generally towards east in both schemes. Furthermore, the water vapor flux of the former scheme is stronger than that of the latter one. The water vapor fluxes are strong over rainfall centers. Figure 7 shows the cross section of water vapor flux divergence along the rainfall center at Litang. In the scheme RAOB, the convergence on 500 hPa is rather strong. It is whole-level convergence to the north of the rainfall center at Litang with divergence right over Litang. There is also convergence-divergence structure in scheme C-TOVS with much weaker intensity than that in scheme RAOB. Above analyses show that with including of satellite data, the data resolution is increased on plateau area, which makes the description of the structure of dynamic systems and moisture status more objective and thus improve efficiently the rainfall

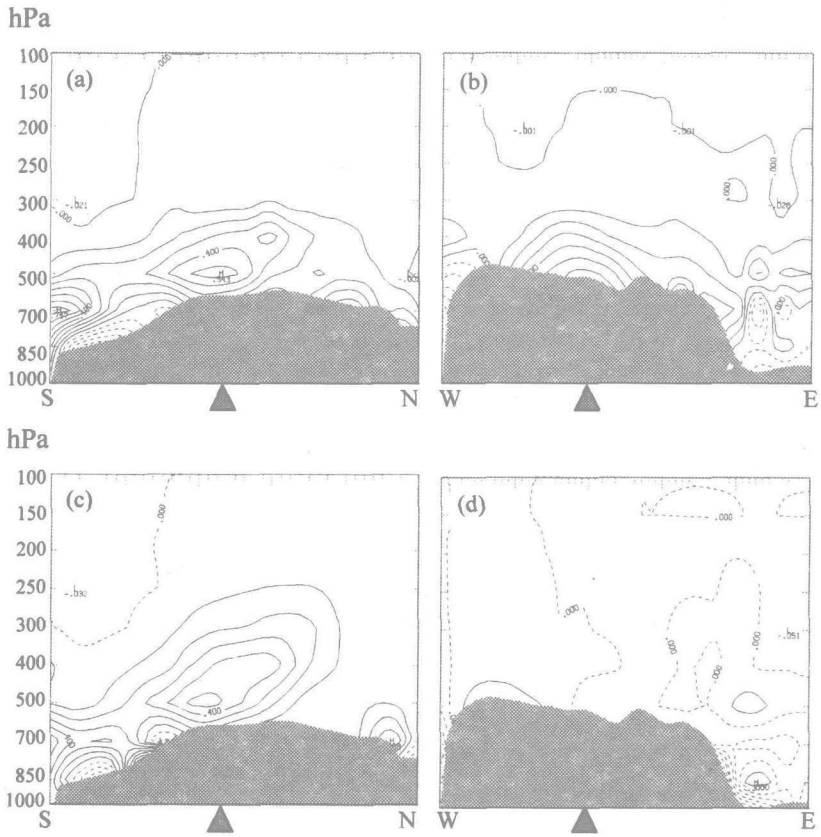

Fig. 6. The cross section of water vapor flux (10^{-3} hPa s^{-1}) along the rainfall center at Litang at 0800 BT 5 July 1995. (Lines SN and WE here are the straight lines in Fig. 4. ▲ denotes the rainfall center at Litang (10^{-3} hPa s^{-1}). (a) and (b) denote scheme RAOB; (c) and (d) denote scheme C-TOVS).

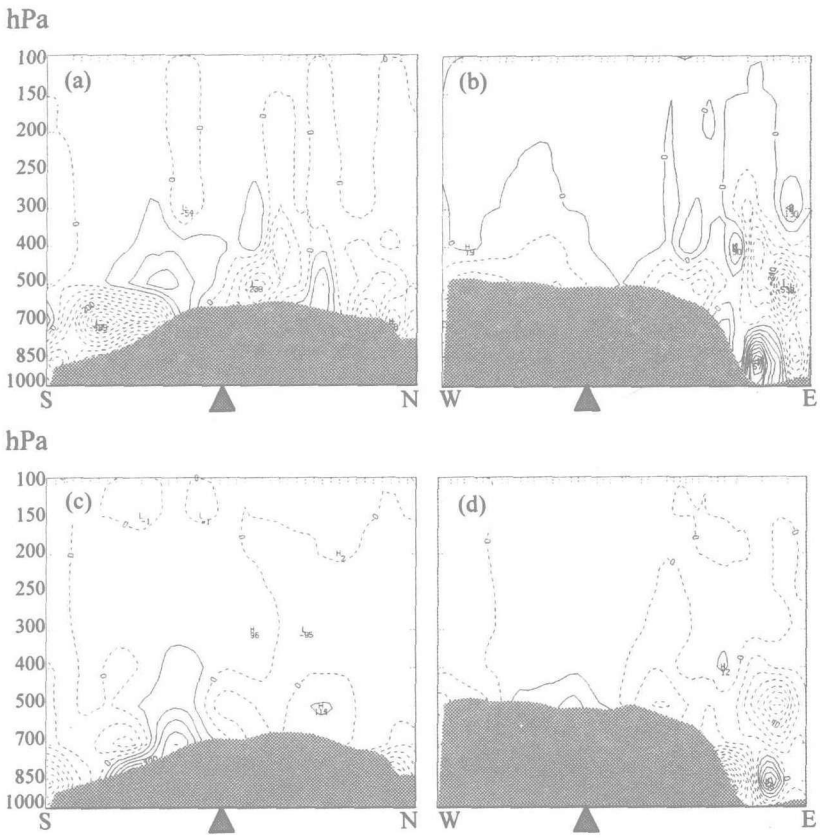

Fig. 7. The cross section of water vapor flux divergence (10^{-3} hPa m s^{-1}) along the rainfall center at Litang at 0800 BT 5 July 1995. (Lines SN and WE here are the lines SN and WE in Fig. 4. ▲ denotes the rainfall center. (a) and (b) denote scheme RAOB; (c) and (d) denote scheme C-TOVS).

forecast of numerical model.

3. *Three-Dimensional Structure of the Vertical Motion and Its Flow Field*

When the moisture condition is satisfied, another condition for moisture condensation has to be met to form the precipitation. The main condition for moisture condensation is vertical motion. Figure 8 shows the cross section of vertical motion along the rainfall center at Litang at 0800 BT 5 July 1995. From the figure, we can see that strong ascending air dominates the whole south-north cross section of scheme RAOB with two ascending centers. The southern center is relevant to the rainfall center at Yuanjiang, Yunnan Province. The other center on the plateau is corresponding to the rainfall center at Litang. The maximum upward motion appears at about 400 hPa, whose value is about -0.646×10^{-3} hPa s^{-1}. In scheme C-TOVS, the maximum upward motion velocity is -0.358×10^{-3} hPa s^{-1}. In the east-west cross section, the ascending motion appears to the eastern part of plateau in scheme RAOB. The maximum upward motion on the plateau appears at about 300 hPa over Litang. In scheme C-TOVS, it is weak descending motion over Litang. The ascending motion appears on both sides of Litang. Figure 9 shows the

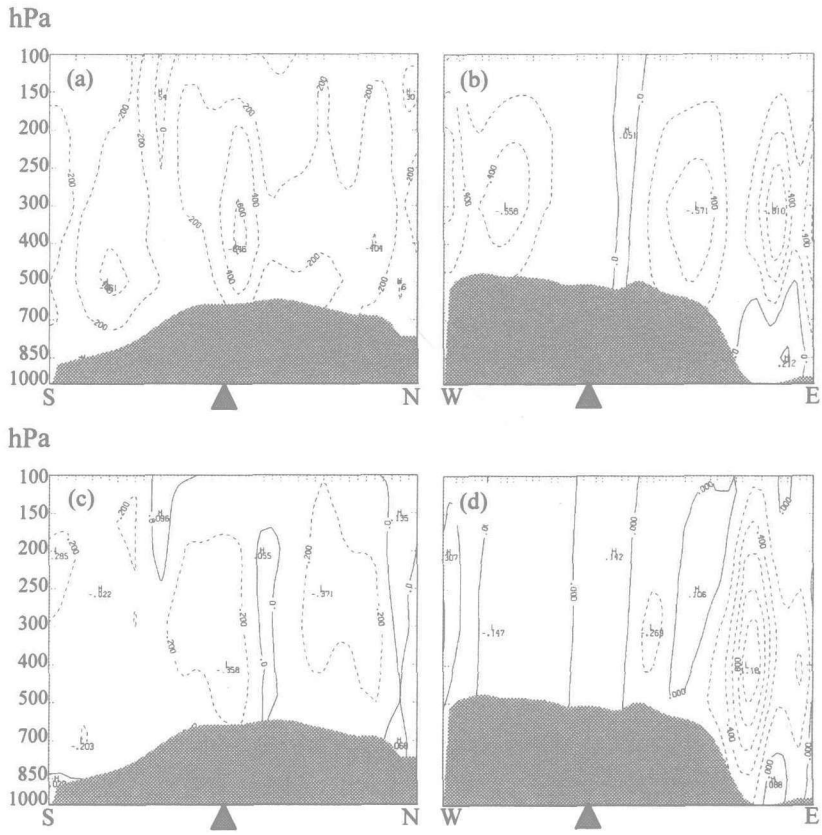

Fig. 8. The cross section of vertical motion (10^{-3}hPa s^{-1}) along the rainfall center at Litang at 0800 BT 5 July 1995. (Lines SN and WE here are the lines SN and WE in Fig. 4. ▲ denotes the rainfall center. (a) and (b) denote scheme RAOB; (c) and (d) denote scheme C-TOVS).

averaged ascending motion in the extent of Litang rainfall area of 270 km×270 km. From this figure, we can see the whole-level ascending motion in scheme RAOB. The averaged maximum velocity appears at 400 hPa. In scheme C-TOVS, it is descending motion below 250 hPa and ascending motion above it. The maximum velocity of the ascending motion of scheme C-TOVS is much smaller than that of scheme RAOB.

Figure 10 shows the cross section of the difference field of vertical and horizontal motions along the rainfall center at Litang between schemes RAOB and C-TOVS. On the cross section of south-north wind and ascending motion in Fig. 10a, it is descending (ascending) motion above 300 hPa to the north (south) of rainfall area. It is descending motion below 300 hPa (the ascending motion in scheme C-TOVS is stronger than that in scheme RAOB, the descending motion is just opposite); On the cross section of west-east wind and ascending motion shown in Fig. 10b, all levels as a whole are dominated by weak ascending motion.

Consequently, the unreal initial information in numerical model on plateau area may lead to the uncertainty in the description of weather system on plateau and its dynamic structure. False vertical motion and its circulation structure may appear. The application of TOVS data can significantly eliminate the false information and improve the capability

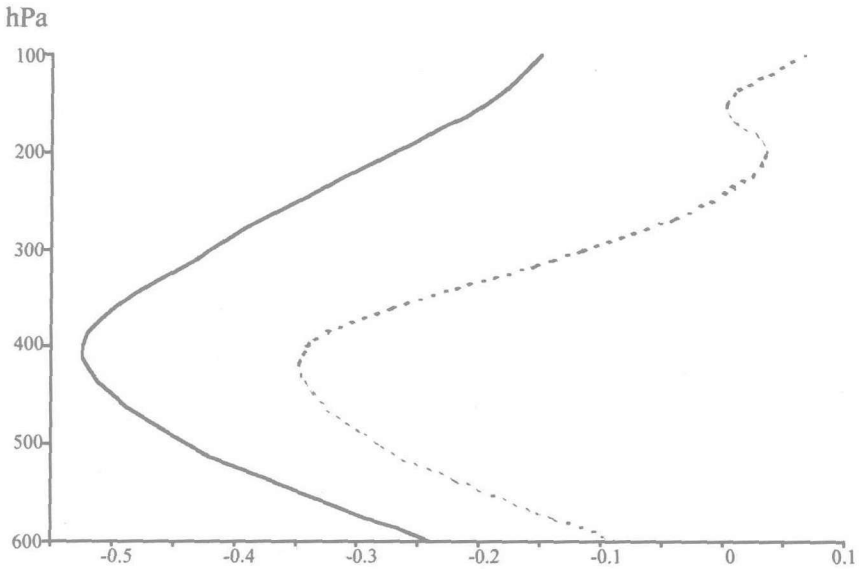

Fig. 9. The averaged ascending motion in the extent of Litang rainfall area of 270 km × 270 km (solid line: scheme RAOB ; dotted line: scheme C-TOVS. unit: 10^{-3}hPa s^{-1}).

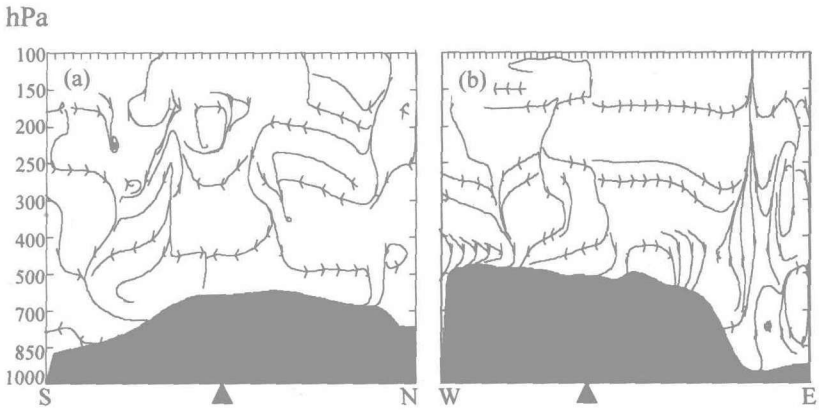

Fig. 10. The cross section of the difference field of vertical and horizontal motions along the rainfall center at Litang between schemes RAOB and C-TOVS (C-TOVS minus RAOB). Horizontal velocity: m s^{-1}; vertical velocity: 10^{-3}hPa s^{-1}. (a) south-north direction; (b) west-east direction.

to describe the three-dimensional physical picture, structure and its dynamic characteristics in the plateau area.

VI. CONCLUSIONS AND DISCUSSION

This paper introduces for the first time TOVS satellite data corrected by variational technique into data-sparse plateau area. From the dynamic theoretic aspect, the improvement on the description of the dynamic and thermodynamic structure features of plateau meteorological field by introducing TOVS data is shown.

(1) Under the geographical condition of the Tibetan Plateau, the observing stations are very sparse, the spatial resolution of data is very low, which would cause false information in the initial field of numerical model. As a result, the description of plateau systems and their dynamic structure would be uncertain. False vertical ascending (descending) motion and its circulation structure features would appear. The feature of the water vapor transportation channel distribution on the plateau and its ambient area would be distorted and reverse effect of water vapor transportation would happen. The correlation between above false information of various variable diagnoses and the distribution of observing stations disclose the problem in numerical prediction technique on plateau area that is difficult to solve.

(2) Study on the application of satellite data on plateau area shows that TOVS satellite data can significantly eliminate above false information in the initial field on the plateau. The capability to describe the three-dimensional physical picture, structure and its dynamic characteristics in plateau area is improved apparently. It is an efficient way to overcome the limitation of sparse observing stations and low spatial data resolution on the plateau.

(3) There exist various system errors in the satellite data on the plateau. The present paper adopts variational correction method and decreases these errors efficiently. The objectivity and reliability of TOVS satellite data application are improved significantly.

REFERENCES

Chen Bomin and Qian Zhengan (1995). Numerical prediction experiments on the rainfall and low vortex on Tibetan Plateau in summer. *Chinese. Atmos Sci.*, **19**: 63—72 (in Chinese).

Wang Zonghao (1995). *Progress in the Application of the Satellite Monitored Heat Radiation in NWP, Some New Techniques in Numerical Weather Prediction (2)*. Beijing. China Meteor. Press. pp. 148—172 (in Chinese).

Xu Xiangde et al. (1996). *Study on the technique to Estimate Rainfall with the Integration of Radar, Satellite and Surface Rain Gauge Tools, Heavy Rain Science*. Beijing. China Meteor. Press. pp. 102—107 (in Chinese).

Zhu Qiangen et al. (1992). *The Principles and Techniques of Synoptic Meteorology*. Beijing. China Meteor. Press. pp. 896—898 (in Chinese).

Zhang D. L., Michael Fritsch J. (1986). Numerical simulation of the meso-β scale structure and evolution of the 1977 Johnstown flood. Part I: model description and verification. *J. Atmos. Sci.*, **43**: 1913—1943.